MATERIALS SCIENCE / МАТЕРИАЛОВЕДЕНИЕ

UDC 621.791.927.5
DOI 10.17073/0368-0797-2025-1-51-59

Original article
Оригинальная статья

Effect of thermal cycles on formation of pearlitic heat-resistant steel structure under wire arc additive manufacturing

I. V. Vlasov ✉, **A. I. Gordienko, V. M. Semenchuk**

Institute of Strength Physics and Materials Science, Siberian Branch of Russian Academy of Sciences (2/4 Akademicheskii Ave., Tomsk 634055, Russian Federation)

✉ viv@ispms.ru

Abstract. The authors investigated the microstructure and mechanical properties of a model wall manufactured by arc wire 3D printing. 3D printing was performed using heat-resistant pearlitic steel wire in coldArc reduced heat input mode. Stationary thermal imager was employed to analyze the thermal cycles during layer deposition. Compressed air cooling to 200 °C was applied before each layer deposition to reduce heat accumulation. The high temperature gradients between the molten metal and the cooled layer resulted in areas with non-uniform structure, typical of welded joints after arc welding. Such areas with non-uniform structure were formed during the printing of each new layer and repeated throughout the wall height. It was observed that each solidified layer undergoes cyclic thermal effects during the deposition of subsequent ten layers. Intensive heating from deposition of two to three new layers leads to partial structural-phase transformations in the underlying layer. Deposition of the next 7 – 8 layers leads to heating similar to the "tempering" thermal operation. Microstructure analysis across different areas of the wall revealed acicular bainite with a small proportion of lath ferrite, bainitic ferrite, and martensitic-austenitic constituents. A slight increase in the width dimensions of acicular structure laths was observed with increasing wall height compared to the lower layers. The highest microhardness values were observed at the wall and substrate fusion zone (320 ± 7 kgf/mm^2) due to rapid heat conduction and high cooling rates during the initial stages of printing. In the wall bulk, microhardness values ranged from 260 to 300 kgf/mm^2. The scatter of values and the periodic nature of the microhardness curve are associated with the formation of areas with non-uniform structure within each deposited layer of the wall. The wall material exhibits high strength characteristics (up to 800 MPa) and relative elongation (9 – 12 %).

Keywords: additive technology, WAAM, GMAW, pearlitic heat-resistant steel, microstructure, mechanical properties, thermal cycling

Acknowledgements: The work was performed within the framework of the Russian Science Foundation project No. 24-29-00827.

For citation: Vlasov I.V., Gordienko A.I., Semenchuk V.M. Effect of thermal cycles on formation of pearlitic heat-resistant steel structure under wire arc additive manufacturing. *Izvestiya. Ferrous Metallurgy*. 2025;68(1):51–59. https://doi.org/10.17073/0368-0797-2025-1-51-59

Влияние термических циклов на формирование структуры жаропрочной стали перлитного класса в условиях проволочного электродугового аддитивного производства

И. В. Власов ✉, **А. И. Гордиенко, В. М. Семенчук**

Институт физики прочности и материаловедения Сибирского отделения РАН (Россия, 634055, Томск, Академический пр., 2/4)

✉ viv@ispms.ru

Аннотация. В работе исследованы микроструктура и механические свойства модельной стенки из жаропрочной стали перлитного класса, изготовленной с использованием электродуговой проволочной 3D-печати в режиме сниженного тепловложения coldArc. Для анализа тепловых циклов при нанесении слоев использовался стационарный тепловизор. Перед нанесением каждого слоя применялось охлаждение сжатым воздухом до 200 °С, чтобы уменьшить накопление тепла. Высокие градиенты температур между расплавленным металлом и охлажденным слоем привели к образованию участков с неоднородной структурой, строение которых типично для сварного шва после электродуговой сварки. Такие участки с неоднородной структурой формируются при печати каждого нового слоя и повторяются по всей высоте стенки. Обнаружено, что каждый закристаллизовавшийся слой подвергается циклическому термическому воздействию при нанесении последующих десяти слоев. Высокий нагрев от нанесения двух-трех новых слоев приводит к частичным структурно-фазовым превращениям в нижележащем слое. Нанесение последующих семи – восьми слоев приводит к нагреву, аналогичному термической

операции отпуск. При анализе микроструктуры в разных участках стенки выявлен игольчатый бейнит с небольшой долей реечного и бейнитного феррита и мартенситно-аустенитной составляющей. По мере увеличения высоты стенки наблюдалось незначительное увеличение ширины реек игольчатых структур по сравнению с нижними слоями стенки. Наиболее высокие значения микротвердости наблюдались в месте сплавления стенки и подложки (320 ± 7 кгс/мм^2) в результате быстрого теплоотвода и высокой скорости охлаждения на начальных этапах печати. В основном объеме стенки значения микротвердости изменялись в диапазоне 260 – 300 кгс/мм^2. Разброс значений и периодический характер кривой микротвердости связан с формированием участков с неоднородной структурой в пределах каждого нанесенного слоя стенки. Материал стенки характеризуется высокими значениями прочностных характеристик (до 800 МПа) и относительного удлинения (9 – 12 %).

Ключевые слова: аддитивная технология, WAAM, GMAW, жаропрочная сталь перлитного класса, микроструктура, механические свойства, термоциклирование

Благодарности: Исследование выполнено за счет гранта Российского научного фонда № 24-29-00827.

Для цитирования: Власов И.В., Гордиенко А.И., Семенчук В.М. Влияние термических циклов на формирование структуры жаропрочной стали перлитного класса в условиях проволочного электродугового аддитивного производства. *Известия вузов. Черная металлургия*. 2025;68(1):51–59. https://doi.org/10.17073/0368-0797-2025-1-51-59

Introduction

Additive manufacturing technologies are categorized into three main groups based on the energy source used: laser-based, electron beam-based, and arc-based methods [1]. Compared to laser- and electron beam-based processes, the use of an electric arc provides higher energy efficiency and greater 3D printing speeds, with material deposition rates reaching approximately 4 – 9 kg/h [2]. A key advantage of wire arc additive manufacturing (WAAM) in a shielding gas environment, based on the *Gas Metal Arc Welding* (GMAW) process, is the ability to produce large-scale components [3]. However, a major disadvantage of WAAM technologies is excessive heat accumulation within the manufactured part [4; 5]. This occurs because heat dissipation becomes more difficult as the number of deposited layers increases [6]. The reduction in cooling rate leads to more complex thermal history during layer deposition, changes in bead width and geometry [7 – 9], and, consequently, results in non-uniform microstructure and property variations across different sections of the part, along with reduced dimensional accuracy.

One approach to mitigating heat accumulation in WAAM is the application of reduced heat input technologies, such as *Cold Metal Transfer* (CMT) (developed by Fronius) and *coldArc* (developed by EWM) [10]. These techniques involve short arc welding, characterized by alternating cycles of short circuiting and arc burning. In [11], it was demonstrated that walls manufactured under reduced heat input conditions exhibit improved mechanical properties and reduced surface roughness. B.P. Nagasai and co-authors [12] identified that components fabricated using CMT technology exhibit a finer-grained microstructure and higher mechanical characteristics compared to those produced under standard arc welding modes in shielding gases.

Monitoring and controlling interlayer temperature (the temperature of the top layer before the next layer is deposited) is another method for managing heat accumulation in the manufactured part. Studies [6; 13] have shown that interlayer temperature increases up to 550 °C as the number of deposited layers grows. To monitor temperature during 3D printing, thermographic infrared cameras [6] or thermocouples [8] are commonly used. To maintain consistent interlayer temperature, the introduction of pauses between layer depositions has been proposed [13; 14]. However, extending the time intervals reduces productivity, as achieving the required interlayer temperature through passive cooling significantly increases the overall manufacturing time. Therefore, active cooling methods are employed to minimize pauses between layers while maintaining geometric accuracy. The simplest and most versatile approach is CO_2 jet cooling, which was investigated in [15] for the production of a titanium alloy wall. However, more complex yet highly efficient cooling systems also exist. In [16], a thermoelectric cooling system was proposed for 3D printing of walls. Its operating principle involves direct heat removal through contact plates that move as the wall grows.

Low-alloy pearlitic heat-resistant steels are an important class of structural steels [17]. These steels are widely used in heat exchangers and steam heaters [18]. The correlation between thermal cycling and microstructural changes (grain morphology and size, phase composition) in pearlitic heat-resistant steels during wire arc additive manufacturing remains insufficiently studied.

Thus, this study aims to investigate the effect of cyclic heating during wire arc additive manufacturing of pearlitic heat-resistant steel on the formation of microstructure and mechanical properties. To minimize heat accumulation in the printed wall and prevent excessive bead spreading during printing, the *coldArc* reduced heat input mode and forced air cooling were applied.

Research materials and methods

For 3D printing of the model wall, a 1.2 mm diameter OK Autrod 13.14 welding wire (ESAB Corporation, USA) with a carbon content of 0.06 – 0.10 % was

used. A 10 mm thick plate of 12Kh1MF steel served as the substrate. According to the quality certificate, the carbon content in 12Kh1MF steel was 0.12 %. This steel has a chemical composition similar to that of the wire and is commonly used for components operating at 540 – 580 °C. The main alloying elements in this steel are chromium, molybdenum, and vanadium.

The 3D printing process was performed using the Gas Metal Arc Welding (GMAW) arc deposition method in a shielding gas environment. The shielding gas consisted of a mixture of 82 % Ar and 18 % CO_2. The movement of the welding torch was controlled using a FANUC AM-100iD robotic arc welding system (FANUC, Japan) with an R-30iB Plus controller. A stationary FLIR A305sc thermal imager was used for temperature monitoring and control.

The manipulator operated in conjunction with an EWM Titan XQ R 400 power source (EWM, Germany). Layer deposition was carried out in the *coldArc* reduced heat input mode, a modification of the GMAW process. The *coldArc* mode allows for reduced heat input by employing short arc welding.

The torch angle relative to the substrate was 10° (Fig. 1, *a*). The 3D printing parameters were as follows: current – 118 A, voltage – 16.9 V, wire feed rate – 3000 mm/min, torch travel speed – 350 mm/min. The wall had a height of approximately 70 mm and consisted of 42 layers (Fig. 1, *b*).

In a previous study [19], the authors investigated the microstructure and mechanical properties of model walls printed using the same wire without additional cooling. It was shown that heat accumulation negatively affects the mechanical properties of the printed walls. In the present study, to reduce heat buildup, each layer was cooled to 200 °C after deposition. Compressed air cooling was applied using a compressor. Additionally, the substrate was preheated to 100 – 150 °C to reduce the temperature gradient and improve fusion zone uniformity.

Samples for mechanical testing and microstructural analysis were extracted from the bulk of the wall. All samples had identical geometry and were polished using abrasive papers of varying grit sizes (80 – 2000) to achieve a mirror-like surface finish. A cross-section of the wall was prepared for microstructural examination and microhardness measurements (Fig. 1, *c*). Microstructure analysis was conducted using a Carl Zeiss Axiovert 25 optical microscope and a LEO EVO 50 scanning electron microscope (Carl Zeiss, Germany) at the NANOTECH Shared Research Facility of the Institute of Strength Physics and Materials Science, Siberian Branch of the Russian Academy of Sciences. Microhardness measurements were taken along the entire height of the cross-section using a PMT-3 microhardness tester with a Vickers pyramid load of 0.98 N (100 g).

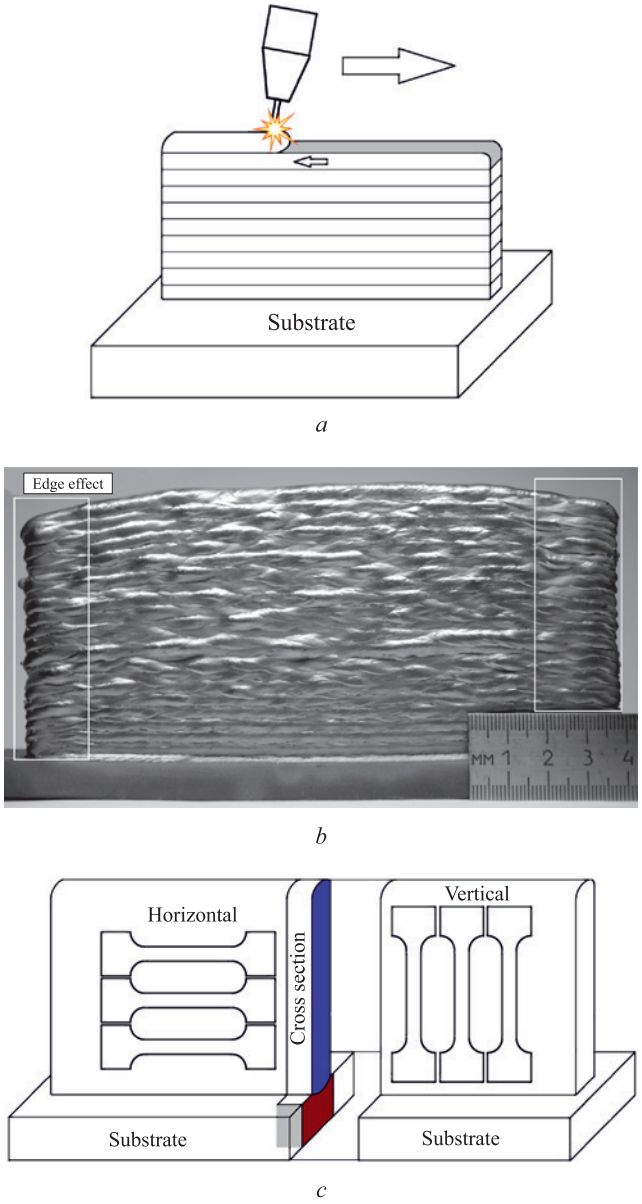

Fig. 1. Schematic representation of layer-by-layer deposition (*a*), appearance of the printed wall (*b*), sample cutting scheme (*c*)

Рис. 1. Схема нанесения слоев (*a*), внешний вид напечатанной стенки (*b*), схема вырезки образцов (*c*)

Tensile test samples had a dog-bone shape (Fig. 1, *c*) with a gauge section of 5×1×30 mm^3. Tensile testing was performed on an Instron 5582 electromechanical testing machine at a crosshead speed of 1 mm/min.

Experiment results

Thermal cycle analysis

Thermal radiation intensity was measured immediately after the deposition of a new layer until the hottest region of the wall cooled down to 200 °C. The measurement results, presented in Fig. 2, *a*, *b*, reflect the thermal evolution following layer deposition and do not

represent the maximum heating values occurring during the 3D printing process.

Thermal imaging was conducted across the entire visible surface of the wall. For ease of data interpretation, two reference points were selected for analyzing temperature variations during wall formation. The locations of these points corresponded to the areas of maximum heating – one at the edges of the lower section of the wall (5th layer), where heat dissipation to the substrate and welding table was high, and another in the middle section of the wall (21st layer). Monitoring the temperature at these points allowed for an assessment of the attenuation of cyclic thermal heating within an individual layer as new layers were deposited on top of it.

At the completion of the fifth layer, the maximum recorded temperature reached ~900 °C (Fig. 2, *a*). The cooling rate of this layer reached 85 °C/s (Fig. 2, *b*).

As subsequent layers were deposited, the peak reheating temperature and cooling rate of the fifth layer gradually decreased. The temperature range necessary for polymorphic transformations (above 700 °C) was reached during the deposition of the sixth and seventh layers (Fig. 2, *a*). The cooling rate at these elevated temperatures decreased to 40 – 50 °C/s. Further layer deposition resulted in heating of the fifth layer to temperatures below 700 °C, which could lead to tempering of the material. When the layer was heated below 700 °C, the cooling rate varied between 10 and 1 °C/s (Fig. 2, *b*).

A similar pattern was observed when analyzing the thermal history of the 21st layer. Heating above 700 °C was achieved during the deposition of the next three layers. Thus, it can be concluded that only the top two to three layers exert a significant thermal effect on the underlying layer, leading to (α → γ) phase transformations.

Metallographic examination

The wall surface exhibits waviness (Fig. 1, *b*), which becomes more pronounced after the deposition of four to six layers. This effect is caused by the spreading behavior of each deposited layer during printing and is characteristic of this manufacturing technology.

Microstructural analysis was performed on a cross-section of the wall (Fig. 1, *c*). At the wall and substrate fusion zone, the fusion boundary and the heat-affected zone (HAZ) are clearly distinguished. A bainitic-martensitic structure formed at the fusion boundary. Moving away from the fusion boundary, the substrate structure within the HAZ transitions from bainitic to ferritic-bainitic, and finally to a ferritic-pearlitic structure in the substrate material.

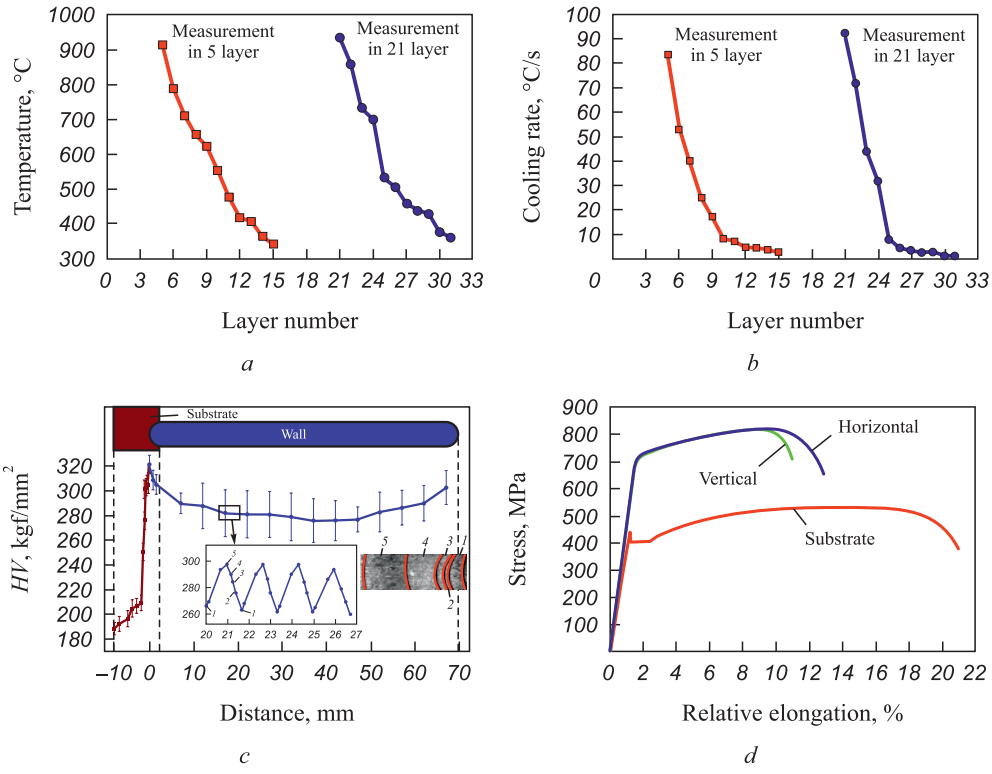

Fig. 2. Changes in temperature (*a*) and cooling rate (*b*) in separate layers during the wall printing, microhardness of the wall cross-section (*c*), graphs of static tension (*d*)

Рис. 2. Изменение температуры (*a*) и скорости охлаждения (*b*) в выбранных слоях в процессе печати стенки, график распределения микротвердости (*c*), диаграммы статического растяжения (*d*)

The wall consists of regions with a non-uniform microstructure (Fig. 3, *a*), which form due to new layer deposition and phase transformations occurring during heating and cooling. Owing to arc oscillation and layer spreading, the height of these regions varies between 1.3 and 2.2 mm. Each region can be divided into five distinct structural zones.

Zone *1* consists of large elongated grains (Fig. 3, *b*), with widths reaching 100 – 150 μm. The grain boundaries correspond to those of the former austenite grains. Within these large grains, a predominantly acicular ferrite (AF) structure is observed. The average width of acicular ferrite laths was 1.78 ± 0.2 μm. In SEM-images, dark interlayers can be observed at grain boundaries, consisting of a matrix with dispersed inclusions ranging in size from 0.18 to 0.70 μm (Fig. 3, *i*).

The microstructure of Zone *2* also contains large grains (Fig. 3, *c*), but they exhibit a quasi-equiaxed shape. In Zone *3*, the grain size with distinct boundaries is significantly smaller, ranging from 17 to 40 μm,

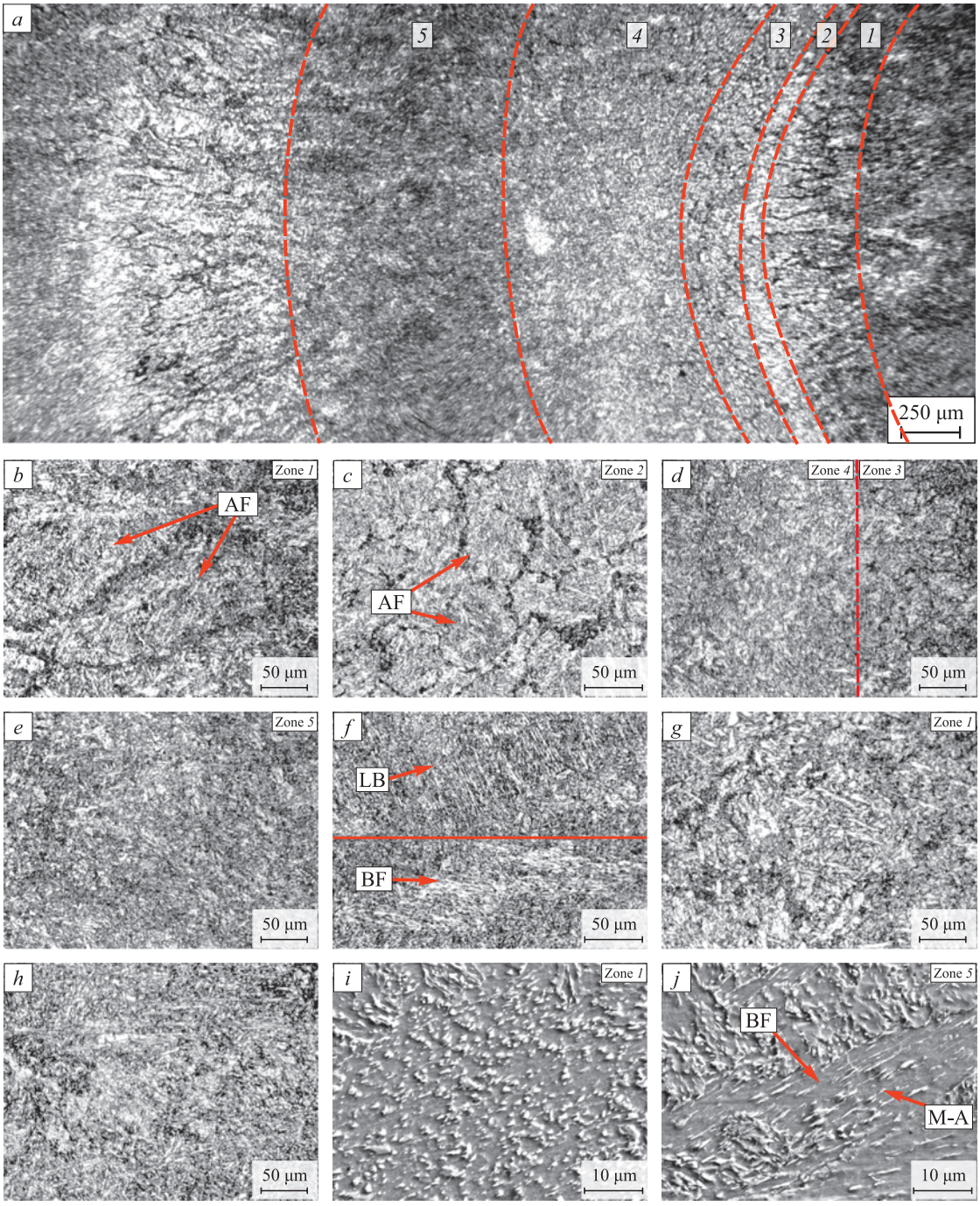

Fig. 3. Optical images of microstructures obtained from the wall cross-section (*a* – *h*), SEM-images (*i*, *j*)

Рис. 3. Оптические изображения микроструктур, полученных с поперечного сечения стенки (*a* – *h*), РЭМ-изображения (*i*, *j*)

and the interlayers at the grain boundaries become thinner (Fig. 3, *d*) compared to Zones *1* and *2*. It appears that the layer boundary is located within Zones *1* and *2*.

Zone *4* consists of a fine-grained ferritic-bainitic structure (Fig. 3, *d*). The size of the quasi-polygonal ferrite grains is 4.41 ± 1.1 μm. The bainitic structure in this zone is represented by acicular ferrite. The prior austenite grain boundaries are no longer distinguishable in Zone *4*.

Zone *5* exhibits the highest refinement of the microstructure and is primarily composed of acicular ferrite (Fig. 3, *e*), with a small proportion of lath bainite (LB) and bainitic ferrite (BF) (Fig. 3, *f*). The average width of acicular ferrite laths in Zone *5* is lower than in Zone *1*, measuring 1.69 ± 0.22 μm. Within bainitic ferrite grains, elongated interlayers are observed, which may correspond to martensitic-austenitic (M–A) constituents (Fig. 3, *j*). Studies [20; 21] indicate that the martensitic-austenitic constituent is a product of incomplete austenite decomposition during bainitic transformation [20; 21]. The width of the martensitic-austenitic interlayers is 0.25 ± 0.11 μm.

As the wall height increases, a slight increase in the width of acicular structure laths is observed, reaching 1.86 ± 0.3 μm in Zone *1* (Fig. 3, *g*) and 1.81 ± 0.44 μm in Zone *5*, compared to the lower layers of the wall (Fig. 3, *b*).

In the upper section of the wall (~5 mm from the top), no distinct regions with characteristic zones are observed. The structure is more uniform and consists of acicular ferrite (Fig. 3, *h*).

Microhardness measurements

The orientation scheme of the wall cross-section for microhardness measurements and the microhardness distribution graphs are presented in Fig. 2, *c*. The fusion boundary between the wall and the substrate is taken as the zero reference point on the *x*-axis. The microhardness curve corresponding to the measurements in the wall lies in the positive range of the *x*-axis, while the microhardness values of the substrate, including the weld-fusion area, fall within the –8 to 2 mm range.

Moving away from the flat surface of the substrate (in contact with the welding table), the microhardness initially increases gradually and then rises sharply. This increase is associated with the thermal effect on the substrate during the deposition of the first layers of the wall. Therefore, the region of sharp microhardness increase corresponds to the HAZ. At the wall and substrate fusion zone, microhardness increases to 320 ± 7 kgf/mm^2 (Fig. 2, *c*). As the number of deposited layers increases, the average microhardness values gradually decrease up to a wall height of ~47 mm (down to ~275 kgf/mm^2), and then increase again to 300 kgf/mm^2 at the top of the wall.

A significant scatter in microhardness values was observed. This variation is attributed to differences in microhardness across regions with non-uniform microstructure (Fig. 3, *a*). A more detailed graph of microhardness variations measured at a distance of 20 mm from the base of the wall is shown in the inset of Fig. 2, *c*. The microhardness values were correlated with corresponding microstructural zones. The highest microhardness values (up to 300 kgf/mm^2) were recorded in Zone *5*, which corresponds to a region with non-uniform microstructure (Fig. 3, *a*). The lowest microhardness values (down to 260 kgf/mm^2) were found in Zone *1*, which is characterized by coarse grains. Zones *2* – *4* exhibit intermediate microhardness values. Since such structurally non-uniform regions are repeated throughout the wall, the microhardness distribution curve exhibits periodicity (Fig. 2, *c*, inset).

Static tensile testing

Fig. 2, *d* presents the loading diagrams for samples extracted from the substrate (12Kh1MF steel) and the printed wall. The loading curve of the substrate samples exhibits a yield plateau, whereas no such plateau is observed in the wall samples. The yield strength and ultimate tensile strength of the wall samples are ~40 and ~34 % higher, respectively, compared to the substrate material, while their ductility is reduced by a factor of two (see Table). The strength characteristics of the wall samples also exceed the mechanical properties of the wire specified in GOST 2246–70 (see Table). The ductility of samples extracted in the vertical direction is ~20 % lower compared to those cut in the horizontal direction.

Discussion of results

The study of thermal cycling during 3D printing of the model wall allowed for an investigation of the effects of diminishing cyclic heating with successive layer deposition and its influence on the microstructure and mechanical properties of the material.

Forced cooling of the wall before depositing a new layer prevented excessive heat accumulation and ensured a high cooling rate for the deposited and underlying layers (Fig. 2, *b*). As a result, regions with a non-uniform structure are present throughout the entire height of the wall (Fig. 3, *a*). While underlying layers undergo reheating, the lower peak temperatures and accelerated cooling limit diffusion processes and recrystallization.

The zones observed within the wall regions (Fig. 3, *a*) correspond to typical zones formed in welded steels. Zone *1* represents the rapid solidification zone from the molten state, as indicated by the presence of large grains elongated in the crystallization direction (Fig. 3, *b*). Zone *2* corresponds to the coarse-grained heat-affected

Results of static tensile test

Результаты испытаний на статическое растяжение

Sample type	Cutting direction	$\sigma_{0.2}$, MPa	σ_v, MPa	ε, %
Substrate	–	410 ± 20*	530 ± 30	20 ± 2
OK Autrod 13.14 Wire (GOST 2246–70)	–	600	700	16
Wall	Horizontal	700 ± 30	800 ± 40	12 ± 2
	Vertical	700 ± 30	810 ± 40	9.5 ± 2
* Yield plateau observed				

zone, where the previous layer was reheated above the austenite recrystallization temperature.

The broad interlayers with internal particles at the boundaries of large grains in Zones *1* and *2* indicate that during thermal cycling, heating reached ($\alpha \rightarrow \gamma$) phase transformation temperatures, allowing for partial diffusion-driven redistribution of carbon at grain boundaries. Due to the lack of prolonged holding time and rapid cooling, intermediate/bainitic structures formed at the grain boundaries.

The reduction in grain size in Zone *3* (Fig. 3, *d*) suggests that this region (fine-grained HAZ) experienced heating above the Ac_3 temperature. In Zone *4*, prior austenite grain boundaries are no longer visible, and a higher proportion of a bright phase with a quasi-equiaxed shape is observed (Fig. 3, *d*). This suggests that heating in this region occurred within the ($\alpha + \gamma$) phase temperature range [22]. Zone *5* experienced the least thermal exposure, both in terms of heating temperature and duration. As a result, this zone retains a microstructure most similar to that formed during the initial solidification of a deposited layer (Fig. 3, *h*).

Thus, during cooling after layer deposition, Zone *1* with large elongated grains forms in the lower portion of the layer, followed by the formation of an acicular ferrite structure in the remaining volume of the layer due to a decrease in cooling rate. Zones *2 – 5* (Fig. 3, *a*) represent heat-affected regions in the previously deposited layer. With the deposition of additional layers, the underlying layers undergo cyclic thermal exposure at varying temperatures (Fig. 2, *a*).

Cooling the wall to 200 °C before depositing a new layer led to higher microhardness values (up to 305 kgf/mm^2, Fig. 2, *c*) compared to air cooling (210 kgf/mm^2), as previously shown in [19]. The decrease in microhardness along the wall height (Fig. 2, *c*) is attributed to thermal cycling and structural "tempering" effects. At the initial stages of printing, the substrate and welding table acted as additional heat sinks, but their influence diminished as the number of layers increased. The formation of a non-uniform structure in the wall resulted in significant microhardness variation. The higher microhardness values in the upper section of the wall are associated with the absence of thermal cycling from subsequently deposited layers (Fig. 2, *c*).

Potential approaches to improving structural uniformity include increasing the preheating temperature before depositing a new layer and optimizing cooling rate ranges to allow sufficient time for recrystallization processes to occur.

Conclusions

The microstructure and mechanical properties of a model wall fabricated using wire arc additive manufacturing in a shielding gas environment under *coldArc* reduced heat input mode were studied.

The use of forced cooling between layer depositions to 200 °C effectively limited heat accumulation in the wall during 3D printing. Due to the high temperature gradient, the cooling rate of the deposited layer reached 85 – 90 °C/s. It was shown that each solidified layer undergoes cyclic thermal exposure during the deposition of the subsequent ten layers. Heating from the deposition of two to three new layers leads to structural-phase transformations in the underlying layer. The next seven to eight layers result in heating comparable to an "tempering" thermal operation.

As a result of rapid cooling after printing, combined with recurrent thermal exposure, regions with non-uniform microstructure formed throughout the entire height of the wall. These regions include: a rapid solidification zone with large elongated grains, a coarse-grained zone, a fine-grained zone, intercritical heat-affected zones.

The microstructure across different areas of the wall consisted primarily of acicular bainite, with a small fraction of lath bainite, bainitic ferrite, and martensitic-austenitic constituents.

A significant scatter in microhardness values was observed along the wall height, ranging from 275 to 320 ± 7 kgf/mm^2, which is attributed to the non-uniform microstructure. The strength properties of the wall material reached 800 MPa, with relative elongation ranging from 9 to 12 %.

References / Список литературы

1. Ding D., Pan Z., Cuiuri D. Wire-feed additive manufacturing of metal components: technologies, developments and future interests. *The International Journal of Advanced Manufacturing Technology*. 2015;81(1–4):465–481. https://doi.org/10.1007/s00170-015-7077-3
2. Buchanan C., Gardner L. Metal 3D printing in construction: A review of methods, research, applications, opportunities and challenges. *Engineering Structures*. 2019;180:332–348. https://doi.org/10.1016/j.engstruct.2018.11.045
3. Jafari D., Vaneker T.H.J., Gibson I. Wire and arc additive manufacturing: Opportunities and challenges to control the quality and accuracy of manufactured parts. *Materials & Design*. 2021;202:109471. https://doi.org/10.1016/j.matdes.2021.109471
4. Chernovol N., Marefat F., Lauwers B., Rymenant P.V. Effect of welding parameters on microstructure and mechanical properties of mild steel components produced by WAAM. *Welding in the World*. 2023;67(4):1021–1036. https://doi.org/10.1007/s40194-022-01422-1
5. Munusamy S., Jerald J. Effect of in-situ intrinsic heat treatment in metal additive manufacturing: A comprehensive review. *Metals and Materials International*. 2023;29:3423–3441. https://doi.org/10.1007/s12540-023-01462-2
6. Rodrigues T.A., Duarte V., Avila J.A., Santos T.G., Miranda R.M., Oliveira J.P. Wire and arc additive manufacturing of HSLA steel: Effect of thermal cycles on microstructure and mechanical properties. *Additive Manufacturing*. 2019;27:440–450. https://doi.org/10.1016/j.addma.2019.03.029
7. Pobol I.L., Bakinovski A.A., Stepankova M.K., Burin A.N., Gubko A.D. Influence of heat cycling conditions in the additive manufacturing of stainless steel and Al–Si alloy raw parts on their microstructure. *Foundry Production and Metallurgy*. 2018;(4):133–138. (In Russ.). https://doi.org/10.21122/1683-6065-2018-4-133-138

   Поболь И.Л., Бакиновский А.А., Степанкова М.К., Бурин А.Н., Губко А.Д. Влияние условий термоциклирования в процессе аддитивного производства заготовок из нержавеющей стали и силумина на их микроструктуру. *Литье и металлургия*. 2018;(4):133–138. https://doi.org/10.21122/1683-6065-2018-4-133-138
8. Zhang T., Li H., Gong H., Wu Y., Chen X., Zhang X. Study on location-related thermal cycles and microstructure variation of additively manufactured inconel 718. *Journal of Materials Research and Technology*. 2022;18:3056–3072. https://doi.org/10.1016/j.jmrt.2022.03.178
9. Vlasov I.V., Gordienko A.I., Kuznetsova A.E., Semenchuk V.M. Structure and mechanical properties anisotropy of a steel product manufactured by layer-by-layer electric arc wire 3D printing. *Izvestiya. Ferrous Metallurgy*. 2023;66(6):709–717. https://doi.org/10.17073/0368-0797-2023-6-709-717

   Власов И.В., Гордиенко А.И., Кузнецова А.Е., Семенчук В.М. Исследование структуры и анизотропии механических свойств стального изделия, полученного методом послойной электродуговой проволочной 3D-печати. *Известия вузов. Черная Металлургия*. 2023;66(6):709–717. https://doi.org/10.17073/0368-0797-2023-6-709-717
10. Cunningham C.R., Flynn J.M., Shokrani A., Dhokia V., Newman S.T. Invited review article: Strategies and processes for high quality wire arc additive manufacturing. *Additive Manufacturing*. 2018;22:672–686. https://doi.org/10.1016/j.addma.2018.06.020
11. Le V.T., Bui M.C., Nguyen T.D., Nguyen V.A., Nguyen V.C. On the connection of the heat input to the forming quality in wire-and-arc additive manufacturing of stainless steels. *Vacuum*. 2023;209:111807. https://doi.org/10.1016/j.vacuum.2023.111807
12. Nagasai B.P., Malarvizhi S., Balasubramanian V. Mechanical properties and microstructural characteristics of wire arc additive manufactured 308 L stainless steel cylindrical components made by gas metal arc and cold metal transfer arc welding processes. *Journal of Materials Processing Technology*. 2022;307:117655. https://doi.org/10.1016/j.jmatprotec.2022.117655
13. Wang T., Zhang Y., Wu Z., Shi C. Microstructure and properties of die steel fabricated by WAAM using H13 wire. *Vacuum*. 2018;149:185–189. https://doi.org/10.1016/j.vacuum.2017.12.034
14. Montevecchi F., Venturini G., Grossi N., Scippa A., Campatelli G. Idle time selection for wire-arc additive manufacturing: A finite element-based technique. *Additive Manufacturing*. 2018;21:479–486. https://doi.org/10.1016/j.addma.2018.01.007
15. Wu B., Pan Z., Ding D., Cuiuri D., Li H., Fei Z. The effects of forced interpass cooling on the material properties of wire arc additively manufactured Ti6Al4V alloy. *Journal of Materials Processing Technology*. 2018;258:97–105. https://doi.org/10.1016/j.jmatprotec.2018.03.024
16. Li F., Chen S., Shi J., Zhao Y., Tian H. Thermoelectric cooling-aided bead geometry regulation in wire and arc-based additive manufacturing of thin-walled structures. *Applied Sciences*. 2018;8(2):207. https://doi.org/10.3390/app8020207
17. Jakubowska M., Wrobel A., Manaj W., Sypien A. Degradation of microstructure and strength properties of heat-resistant steels operating under variable loads. *International Journal of Pressure Vessels and Piping*. 2023;202:104916. https://doi.org/10.1016/j.ijpvp.2023.104916
18. Zhang J., Chen H., Fan D., Huang J., Yu X., Feng W., Xu K. Effects of phosphorus impurity on the microstructure and impact toughness of weld joint for the 12Cr2Mo1R heat resistant steel. *Journal of Manufacturing Processes*. 2019; 38:453–461. https://doi.org/10.1016/j.jmapro.2019.01.026
19. Vlasov I.V., Gordienko A.I., Eremin A.V., Semenchuk V.M., Kuznetsova A.E. Structure and mechanical behavior of heat-resistant steel manufactured by multilayer arc deposition. *Metals*. 2023;13(8):1375. https://doi.org/10.3390/met13081375
20. Sridharan N., Noakes M.W., Nycz A., Love L.J., Dehoff R.R., Babu S.S. On the toughness scatter in low alloy C–Mn steel samples fabricated using wire arc additive manufacturing. *Materials Science and Engineering: A*. 2018;713:18–27. https://doi.org/10.1016/j.msea.2017.11.101
21. Shi Y., Han Z. Effect of weld thermal cycle on microstructure and fracture toughness of simulated heat-affected zone for a 800 MPa grade high strength low alloy steel. *Journal of Materials Processing Technology*. 2008;207(1–3):30–39. https://doi.org/10.1016/j.jmatprotec.2007.12.049

22. Poletskov P.P., Denisov S.V., Nikitenko O.A., Chukin D.M., Gushchina M.S. Decay of supercooled austenite of low-carbon pipe steel with the use of Gleeble 3500 complex. *Izvestiya. Ferrous Metallurgy*. 2019;62(3):235–240. (In Russ.).
https://doi.org/10.17073/0368-0797-2019-3-235-240

Полецков П.П., Денисов С.В., Никитенко О.А., Чукин Д.М., Гущина М.С. Исследование распада переохлажденного аустенита низкоуглеродистой трубной стали с использованием комплекса Gleeble 3500. *Известия вузов. Черная металлургия*. 2019;62(3):235–240.
https://doi.org/10.17073/0368-0797-2019-3-235-240

Information about the Authors / Сведения об авторах

Il'ya V. Vlasov, *Cand. Sci. (Eng.), Research Associate of the Laboratory of Physical Mesomechanics and Non-Destructive Testing*, Institute of Strength Physics and Materials Science, Siberian Branch Russian Academy of Sciences
ORCID: 0000-0001-9110-8313
E-mail: viv@ispms.ru

Antonina I. Gordienko, *Cand. Sci. (Eng.), Research Associate of the Laboratory of Physical Mesomechanics and Non-Destructive Testing*, Institute of Strength Physics and Materials Science, Siberian Branch Russian Academy of Sciences
ORCID: 0000-0002-4361-8906
E-mail: mirantil@ispms.ru

Vyacheslav M. Semenchuk, *Junior Researcher of the Laboratory of Local Metallurgy in Additive Manufacturing Technologies*, Institute of Strength Physics and Materials Science, Siberian Branch Russian Academy of Sciences
ORCID: 0000-0002-7215-0505
E-mail: svm_70@ispms.ru

Илья Викторович Власов, *к.т.н., научный сотрудник лаборатории физической мезомеханики и неразрушающих методов контроля*, Институт физики прочности и материаловедения Сибирского отделения РАН
ORCID: 0000-0001-9110-8313
E-mail: viv@ispms.ru

Антонина Ильдаровна Гордиенко, *к.т.н., научный сотрудник лаборатории физической мезомеханики и неразрушающих методов контроля*, Институт физики прочности и материаловедения Сибирского отделения РАН
ORCID: 0000-0002-4361-8906
E-mail: mirantil@ispms.ru

Вячеслав Максимович Семенчук, *младший научный сотрудник лаборатории локальной металлургии в аддитивных технологиях,* Институт физики прочности и материаловедения Сибирского отделения РАН
ORCID: 0000-0002-7215-0505
E-mail: svm_70@ispms.ru

Contribution of the Authors / Вклад авторов

I. V. Vlasov – formation of the main concept, goals and objectives; writing the text, literary review, conducting mechanical tests, data analysis.

A. I. Gordienko – performing microstructural studies, results processing, data analysis, revising the text.
V. M. Semenchuk – selection of additive manufacturing modes, preparation of the samples, results discussion.

И. В. Власов – формирование основной концепции, цели и задач исследования; написание текста статьи, литературный обзор публикаций по теме, проведение механических испытаний, анализ экспериментальных данных.
А. И. Гордиенко – проведение микроструктурных исследований, обработка результатов и анализ данных, доработка текста.
В. М. Семенчук – подбор режимов проведения аддитивного формования, подготовка образцов для исследований, обсуждение полученных результатов.

Received 15.05.2024
Revised 05.06.2024
Accepted 12.11.2024

Поступила в редакцию 15.05.2024
После доработки 05.06.2024
Принята к публикации 12.11.2024